

The Tunable Electronic, Magnetic and Curie Temperature by Co Doping $\text{Fe}_{2-x}\text{Co}_x\text{MnAl}$ Alloys

XIAO-PING WEI^{a,*}, SHENG-MING MA^a, XIAO-WEI SUN^a, PEIFENG GAO^b
AND YA-LING ZHANG^c

^aThe School of Mathematics and Physics, Lanzhou Jiaotong University, Lanzhou 730070, P.R. China

^bKey Laboratory of Mechanics on Western Disaster and Environment, MoE,
College of Civil Engineering and Mechanics, Lanzhou University, Lanzhou 730000, P.R. China

^cInstitute of Modern Physics, Chinese Academy of Sciences, Lanzhou 730000, P.R. China

(Received May 10, 2019; revised version July 22, 2019; in final form August 5, 2019)

Using the spin-polarized relativistic Korringa–Kohn–Rostoker method, we study the electronic, magnetic, and Curie temperature of $\text{Fe}_{2-x}\text{Co}_x\text{MnAl}$ alloys. Results indicate that the $\text{Fe}_{2-x}\text{Co}_x\text{MnAl}$ alloys preserve the ferromagnetic metallic nature, and the spin polarization is close to 80% when the Co concentration attains to 30%. The calculated total magnetic moment increases linearly as the increase of Co doping concentration, only small changes are observed for Fe(A), Mn(B), and Fe(C) atomic magnetic moments, while for the Al atom, the magnetic moment always nearly approach to zero. The Heisenberg exchange calculations imply that the Co(A)–Mn(B) exchange plays a leading role in interactions, in contrast to the Mn(B)–Mn(B) exchange in pure Fe_2MnAl . We further calculate the sum of exchange coupling parameters between the constituents, and evaluate the Curie temperature of $\text{Fe}_{2-x}\text{Co}_x\text{MnAl}$ alloys. It is found that the Mn(B)–Mn(B) and Fe/Co(A)–Mn(B) coupling parameters increase evidently with the increase of Co content, and then leading to the Curie temperature above room temperature when the Co doping concentration is over 60%, the change is also in good consistence with calculated total magnetic moment.

DOI: [10.12693/APhysPolA.136.520](https://doi.org/10.12693/APhysPolA.136.520)

PACS/topics: 71.20.Lp, 74.20.Pq, 51.60.+a, 71.70.Gm

1. Introduction

The Heusler alloys, which are firstly discovered by Heusler from the Cu_2MnAl behaving like ferromagnet, although its constituent elements itself are not magnetic [1], have attracted wide attention because of their potential applications in cutting edge technology in spintronics [2–7]. Particularly, the Heusler alloys with high Curie temperature and high spin polarization are more favorable in realistic applications. However, some cheaper and more promising Heusler alloys do not show these interesting physical properties. In this case, we usually tune their electron density to achieve the physical properties of interest such as high Curie temperature and high spin polarization through an appropriate choice of substitutional doping meanwhile retaining their essential structures [8–11].

Recently, Fe_2Mn -based Heusler alloys have drawn widespread attention from both theoretical and experimental aspects [12–17]. Especially, Fe_2MnZ ($Z = \text{Sn}, \text{Al}, \text{Si}$) alloys have been synthesized in experiment [18–20]. Among these alloys, Fe_2MnAl is promising material since it is made up of common elements, which makes it possible to be widely used in various spintronics devices. However, a lower Curie

temperature and spin polarization limit its application in room temperature spintronics devices [16, 17].

In this work, we will take Fe_2MnAl as the object of study, and tune its electron density by doping Co at Fe(A) site in the series of $\text{Fe}_{2-x}\text{Co}_x\text{MnAl}$ alloys in order to obtain interesting physical properties such as high Curie temperature and high spin polarization, etc. This research can broaden the application scope of Fe_2MnAl . We also can understand the inherent physical mechanism resulting in the changes of the Curie temperature and spin polarization of Fe_2MnAl , and then providing a feasibility for the improvement of the physical properties of such alloys.

More specifically, the paper is organized as follows. Calculation details are given in Sect. 2, followed by the results and discussion in Sect. 3. Finally, we present a conclusion in Sect. 4.

2. Calculation details

In current calculations, we use the coherence potential approximation within spin-polarized scalar relativistic Korringa–Kohn–Rostoker package Munich SPRKKR [21]. The exchange–correlation potential was modeled by using the Perdew–Burke–Ernzerhof (PBE) parametrization in scheme of the generalized gradient approximations (GGA) [22]. An angular momentum cut-off of $l_{\text{max}} = 3$ and $22 \times 22 \times 22$ k -point mesh in the irreducible wedge of the Brillouin zone are used in calculations.

*corresponding author; e-mail: weixp2008@gmail.com

By using the exchange coupling parameters J_{ij} , we calculate the Curie temperature with mean-field approximation (MFA). In the classical Heisenberg model, the Hamiltonian of a spin system is given by

$$H = - \sum_{i,j} e_i e_j J_{ij}, \quad (1)$$

with the Heisenberg pair exchange coupling parameters J_{ij} , and unit vectors e_i (e_j) pointing in the direction of the magnetic moment on site i (j). The Heisenberg exchange coupling parameter J_{ij} were calculated via the Liechtenstein–Katsnelson–Antropov–Gubanov (LKAG) formalism as [23]:

$$J_{ij} = \frac{1}{\pi} \int_{-\infty}^{\varepsilon_F} \text{Im} \left[\text{Tr} (\Delta_i \tau_{ij}^\uparrow \Delta_j \tau_{ji}^\downarrow) \right] d\varepsilon, \quad (2)$$

where $\Delta_i = t_{i,\uparrow}^{-1} - t_{i,\downarrow}^{-1}$ is the spin-resolved difference of single-site scattering matrix t_i at site i , and τ_{ij} is the scattering path operator, describing the propagation of the electrons between two sites i and j . The Fermi energy is denoted by ε_F . According to J_{ij} , the Curie temperature can be estimated within the MFA. More detailed calculations on the Curie temperature can be seen in our previous works [24, 25]. In MFA, we construct a 4×4 matrix to obtain the Curie temperature, and adopt pair exchange coupling parameters up to $r_{max} = 4.0$ a.u. It needs to be stressed that the atomic J_{ij} of A site with other atoms equals to the sum of J_{ij}^{Fe} and J_{ij}^{Co} .

3. Results and discussion

3.1. Equilibrium states and lattice parameters

Initially, we build structural model of a series of $\text{Fe}_{2-x}\text{Co}_x\text{MnAl}$ alloys based on Fe_2MnAl which has been confirmed in experiment crystallizing in the $L2_1$ structure [13]. In the structure, the Fe atoms occupy A(0,0,0) and C($\frac{1}{2}, \frac{1}{2}, \frac{1}{2}$) Wyckoff position, and the Mn and Al atoms are located on B($\frac{1}{4}, \frac{1}{4}, \frac{1}{4}$) and D($\frac{3}{4}, \frac{3}{4}, \frac{3}{4}$) positions, respectively. Among these positions, the Fe atom located at A site is partially substituted by Co element. In order to obtain the equilibrium states of $\text{Fe}_{2-x}\text{Co}_x\text{MnAl}$ alloys at different Co doping concentration, we fit the volume-energy data by using the Murnaghan equation [26]. The fitted equilibrium parameters are tabulated in Table I. From Table I, we notice that the total energies of doped systems are much lower than pure Fe_2MnAl , indicating that they are possible to be synthesized in experiment. In addition, other available theoretical and experimental values are also given for comparison, it is obvious that our results are well consistent with others [8, 14, 17, 27].

3.2. Density of states and magnetic moments

Based on the equilibrium states, we calculate the density of states (DOS) of $\text{Fe}_{2-x}\text{Co}_x\text{MnAl}$ alloys, and show them in Fig. 1. From these calculated DOS, we notice

TABLE I

The calculated lattice parameter (a in Å), bulk modulus (B_0 in GPa), total energy (E_{tot} in Ry) and Curie temperature (T_C in K) for $\text{Fe}_{2-x}\text{Co}_x\text{MnAl}$ alloys.

x	a_{calc}	a_{calc}	a_{exp}	B_0	E_{tot}	T_C
0.0	5.618	5.680 ^a (5.62 ^c)	5.816 ^b	187.4	-7894.32	4.24
0.1	5.613	–	–	166.3	-7918.45	109.32
0.2	5.618	–	–	182.7	-7942.59	155.88
0.3	5.628	–	–	168.7	-7966.73	205.91
0.4	5.621	–	–	207.0	-7990.86	245.72
0.5	5.626	5.63 ^c	–	197.3	-8015.00	281.58
0.6	5.632	–	–	195.4	-8039.13	313.02
0.7	5.663	–	–	218.3	-8063.27	341.75
0.8	5.665	–	–	213.2	-8087.41	367.24
0.9	5.634	–	–	168.9	-8111.55	392.00
1.0	5.669	5.692 ^d	5.786 ^d	305.8	-8135.69	384.65

^aRef. [14], ^bRef. [17], ^cRef. [8], ^dRef. [27]

that the transition metal $3d$ states offer a main contribution to total DOS for a series of $\text{Fe}_{2-x}\text{Co}_x\text{MnAl}$ alloys, and the $d-d$ orbital hybridization plays a main role around the Fermi level. In addition, the spin-up states occupy majority-spin states compared with spin-down states, and then the $\text{Fe}_{2-x}\text{Co}_x\text{MnAl}$ alloys are ferromagnets, and indicates the metallic behaviour since the Fermi level goes through the both spin-up and spin-down DOS. The Fermi level is pushed to pseudogap of spin-up states when Co dopant is in a 0.1–0.4 range, and deviate from the pseudogap with the further increase of Co doping concentration. It is due to the decrease of exchange splitting of $d-d$ hybridization states. It is also shown by spin polarization in Fig. 2, that the spin polarization is increasing when Co content increases within $x \leq 0.4$. Particularly, the spin polarization nearly closes to 80% when $x = 0.4$. In addition, we also note that the polarization is always above 40% at different Co doping concentration. With more details, from the calculated total magnetic moments as shown in Table II, we notice that the total magnetic moments of $\text{Fe}_{2-x}\text{Co}_x\text{MnAl}$ alloys nearly obey the Slater–Pauling rule $M_t = Z_t - 24$ [28, 29], where M_t is the calculated total magnetic moment, and Z_t is the valence electrons number per formula unit. Small deviation from integer is ascribed to adopted KKR method. $\text{Fe}_{2-x}\text{Co}_x\text{MnAl}$ alloys are not half-metals due to the conduction electrons at the Fermi level unpolarized fully. It is also confirmed by calculated DOS and spin polarization in Figs. 1 and 2.

In addition, we also notice that the Mn(B) atom offers a main contribution to total magnetic moment. The dependences of magnetic moments on Co doping concentration are presented in Fig. 3. It can be seen that total magnetic moment increases almost linearly with the increase of Co doping content, the change is attributed to the increase of the Mn(B) and Co(A) atomic moments. In contrast, small change is observed for the magnetic moments of Fe atoms. For the Al atom, the magnetic moment nearly becomes zero because of the Al unpolarized atom.

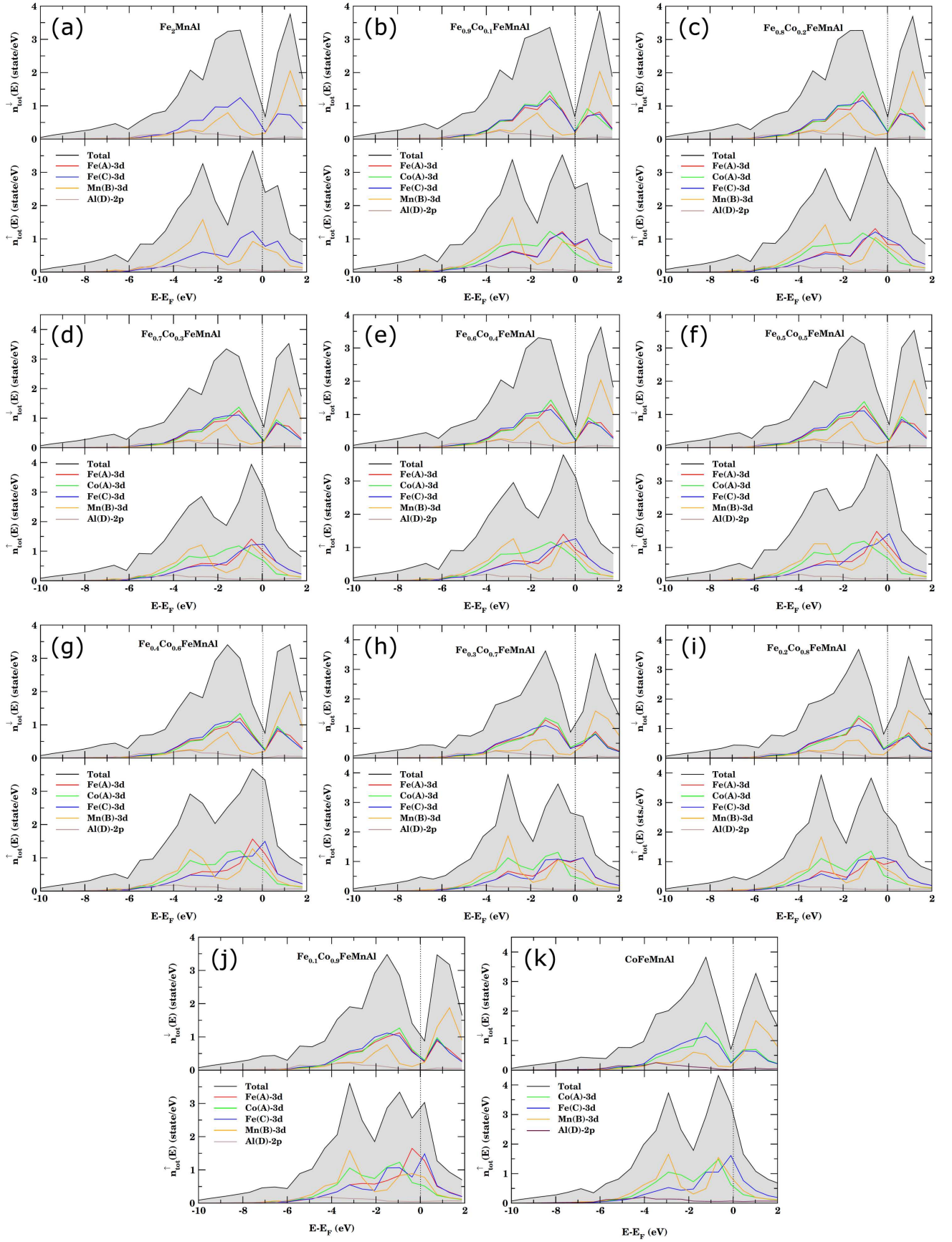


Fig. 1. Total and resolve density of states for a series of $\text{Fe}_{2-x}\text{Co}_x\text{MnAl}$ alloys.

Total and atomic magnetic moments (in μ_B units) of $\text{Fe}_{2-x}\text{Co}_x\text{MnAl}$ alloys are tabulated and compared with available results by reference.

TABLE II

x	M_{calc}	M_{calc}	Fe(A)	Co(A)	Fe(C)	Mn(B)	Al(D)
0.0	2.00	2.01 ^a	-0.20 (-0.27 ^a)	–	-0.20 (-0.27 ^a)	2.44 (2.29 ^a)	-0.04 (-0.01 ^a)
0.1	2.10	–	-0.12	0.59	-0.24	2.44	-0.04
0.2	2.20	–	-0.10	0.65	-0.28	2.47	-0.04
0.3	2.30	–	-0.09	0.70	-0.30	2.50	-0.05
0.4	2.40	–	-0.09	0.73	-0.29	2.51	-0.05
0.5	2.51	2.50 ^a	-0.09	0.75	-0.30	2.53	-0.06
0.6	2.61	–	-0.09	0.76	-0.30	2.55	-0.06
0.7	2.71	–	-0.11	0.77	-0.35	2.62	-0.07
0.8	2.80	–	-0.11	0.78	-0.35	2.63	-0.07
0.9	2.90	–	-0.10	0.79	-0.31	2.59	-0.08
1.0	2.98	3.00 ^a	–	0.79 (0.81 ^a)	-0.40 (-0.14 ^a)	2.67 (2.44 ^a)	-0.08 (-0.04 ^a)

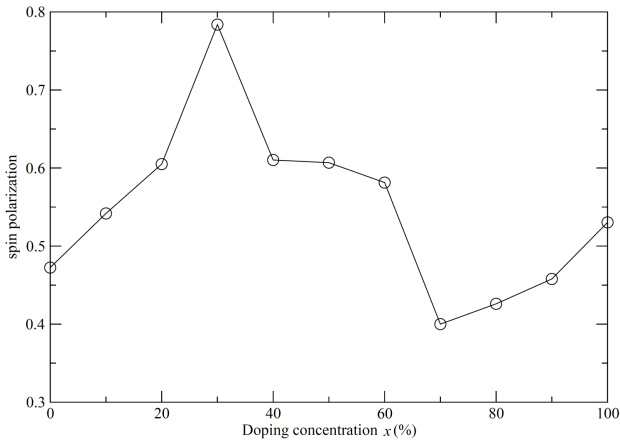
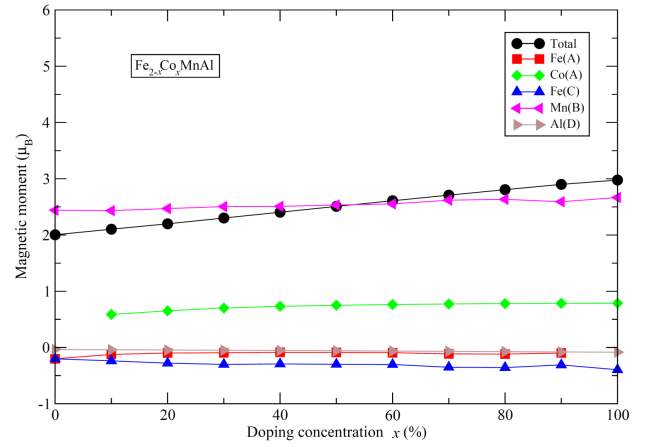
^aRef. [8]

Fig. 2. Spin polarization at different Co doping concentration.

3.3. Exchange interactions and Curie temperatures

In Fig. 4, we show the calculated Heisenberg exchange coupling parameters J_{ij} . It is evident that the exchange interactions are tightly restricted to clusters of radius $r \leq 2.0a$. Specifically, the intra-sublattice Mn(B)–Mn(B) interaction provides significant contribution in overall interactions in Fe_2MnAl , and the interaction between the first nearest neighbor and second nearest neighbor is ferromagnetic, and the third nearest neighbor is antiferromagnetic interaction. The inter-sublattices Fe(A)–Mn(B) and Fe(C)–Mn(B) as well as intra-sublattice Fe(A)–Fe(C) exchanges between the first and second nearest neighbor are ferromagnetic, and the sum of J_{ij} is rather small, approaching nearly zero. For the $\text{Fe}_{0.9}\text{Co}_{0.1}\text{FeMnAl}$ alloy, the inter-sublattice Co(A)–Mn(B) exchange plays a leading role in all interactions, followed by the intra-sublattice Mn(B)–Mn(B). The inter-sublattice Co(A)–Mn(B) exchange between the first nearest neighbor and second nearest neighbor is antiferromagnetic interaction. In contrast, it is ferromagnetic interaction for the intra-sublattice Mn(B)–Mn(B)

Fig. 3. Total and atomic magnetic moments on different Co doping concentration for a series of $\text{Fe}_{2-x}\text{Co}_x\text{MnAl}$ alloys.

exchange. In $\text{Fe}_{0.8}\text{Co}_{0.2}\text{FeMnAl}$ alloy, the situation is the same as in the case of $\text{Fe}_{0.9}\text{Co}_{0.1}\text{FeMnAl}$, the difference is that the ferromagnetic interaction is stronger. In the $\text{Fe}_{0.7}\text{Co}_{0.3}\text{FeMnAl}$ alloy, the inter-sublattice Co(A)–Mn(B) and Fe(C)–Mn(B) interactions become further stronger between the first nearest neighbor and second nearest neighbor, and the intra-sublattice Mn(B)–Mn(B) exchange between the first and second nearest neighbor are smaller. Further, the ferromagnetic exchanges of inter-sublattices Co(A)–Mn(B) and Fe(C)–Mn(B) further increase with the increase in Co doping concentration. It needs to be emphasized that the interactions with Al are omitted, because it is close to zero for all distances. In the $\text{Fe}_{1-x}\text{Co}_x\text{FeMnAl}$ alloys, the J_{ij} shows a oscillatory behavior with increase in interatomic distances r , implying a RKKY exchange [30]. Finally, the behavior disappears with increase in interatomic distance. In addition, we also offer the sum of J_{ij} in Fig. 5, where it can be seen that the sum of intra-sublattices

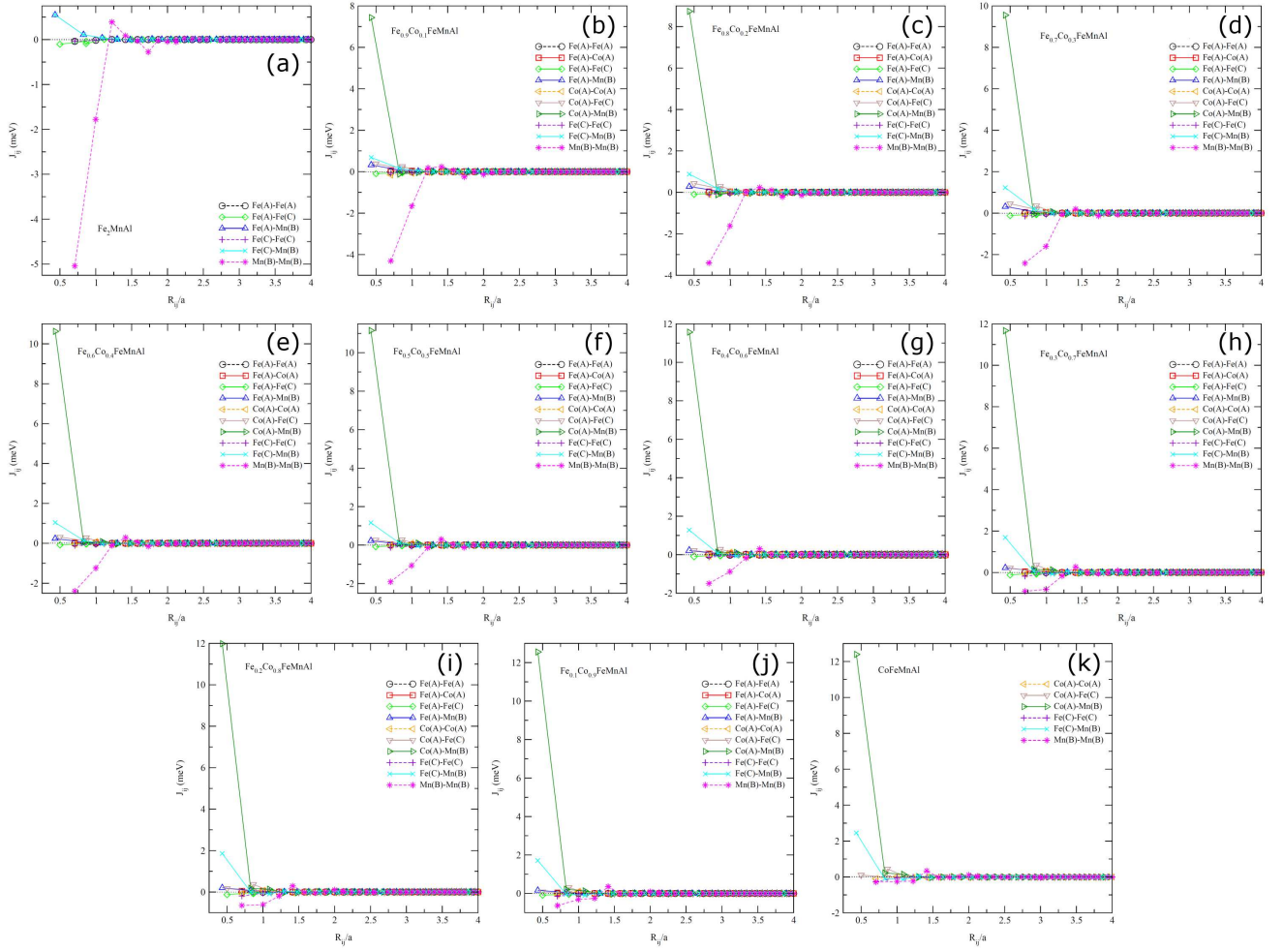


Fig. 4. Heisenberg exchange coupling parameters J_{ij} for a series $\text{Fe}_{2-x}\text{Co}_x\text{MnAl}$ alloys as a function of the interatomic distance r .

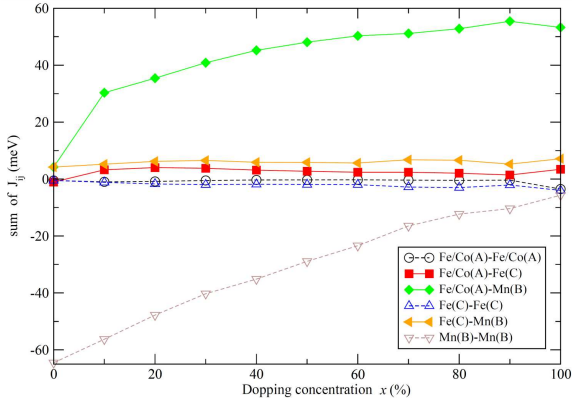


Fig. 5. Sum of exchange interaction J_{ij} between different sites for a series of $\text{Fe}_{2-x}\text{Co}_x\text{MnAl}$ alloys.

$\text{Fe(C)}\text{-Fe(C)}$ and $\text{Fe/Co(A)}\text{-Fe/Co(A)}$ exchange is nearly zero. For the inter-sublattices $\text{Fe/Co(A)}\text{-Fe(C)}$ and $\text{Fe(C)}\text{-Mn(B)}$ exchange, the sum of coupling parameters are about 5 meV and 8 meV, respectively. For the inter-sublattice $\text{Fe/Co(A)}\text{-Mn(B)}$ exchange, the sum of J_{ij} is

gradually increasing as the increase of Co doping concentration, and approaching to 55 meV at $x = 0.8$. For the intra-sublattice $\text{Mn(B)}\text{-Mn(B)}$ exchange, the sum of J_{ij} hardly increases linearly, and the value is largest at $x = 0$, up to 65 meV. Actually, a negative J_{ij} implies that the interaction acts against the ferromagnetic order on this lattice and reduces the Curie temperature. By contrast, a positive J_{ij} can improve the Curie temperature.

Based on the exchange coupling parameters described above, we calculate the Curie temperature for different Co doping concentration by the MFA, and show them in Table I. In Figure 6, we also show the calculated Curie temperature dependence in the Co doping concentration. It is found that the Curie temperature is increasing with the increase of Co doping concentration. The Curie temperature is up to 313.02 K when the Co doping concentration is up to $x = 0.6$, and further increase with the increase of Co doping concentration, finally reaching 392.00 K when $x = 0.9$, which is evidently above room temperature, indicating their potential magnetic applications. By comparing with Fig. 3, we

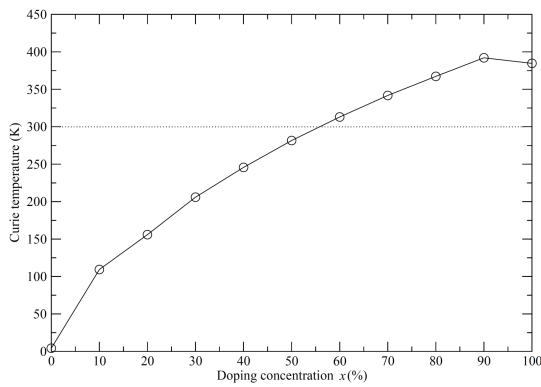


Fig. 6. Curie temperature as a function of different Co doping concentration. Note that the dotted line represents the room temperature.

observe that the Curie temperatures of $Fe_{2-x}Co_xMnAl$ alloys are roughly proportional to the total magnetic moment.

4. Summary and conclusion

We have performed the electronic, magnetic, and Curie temperature calculations on the $Fe_{2-x}Co_xMnAl$ alloys with $L2_1$ structure by using the SPRKKR method. It is found that the $Fe_{2-x}Co_xMnAl$ alloys are ferromagnets and show metallic behavior. However, the calculated total magnetic moments nearly obey the Slater–Pauling rule. The Mn(B) atomic magnetic moment is increasing with the increase of Co doping concentration. Only small change is observed for the moments of Fe atoms, the magnetic moment of unpolarized Al atom is nearly zero. From the calculated exchange interactions, it is found that the inter-sublattice Fe/Co(A)–Mn(B) exchange plays a leading role in all interactions, and finally determines the Curie temperature. Further, we estimate the Curie temperatures of different Co doping concentration by using MFA. Results indicate that the Curie temperature is above room temperature when the Co doping concentration is over 60%. More noticeably, the Curie temperatures of $Fe_{2-x}Co_xMnAl$ alloys are roughly proportional to the total magnetic moment. We hope that the study can provide some valuable hints for further performance improvement of such alloys.

Acknowledgments

The project is supported by National Natural Science Foundation of China (No. 11864021). The work is also supported by Foundation of A Hundred Youth Talents Training Program of Lanzhou Jiaotong University. Peifeng Gao would like to acknowledge the supports by the China Postdoctoral Science Foundation (No. 2018M633604) and the Fundamental Research Funds for the Central Universities (No. lzujbky-2018-it01).

References

- [1] F. Heulser, *Verhandl. Deut. Physik. Ges.* **5**, 219 (1903).
- [2] L. Bainsla, K.G. Suresh, *Appl. Phys. Rev.* **3**, 031101 (2016).
- [3] B. Dieny, V.S. Speriosu, S.S.P. Parkin, B.A. Gurney, D.R. Wilhoit, D. Mauri, *Phys. Rev. B* **43**, 1297 (1991).
- [4] S.A. Wolf, D.D. Awschalom, R.A. Buhrman, J.M. Daughton, S.V. Molnar, M.L. Roukes, A.Y. Chtchelkanova, D.M. Treger, *Science* **294**, 1488 (2001).
- [5] S.S.P. Parkin, M. Hayashi, L. Thomas, *Science* **320**, 190 (2008).
- [6] O. Gutfleisch, M.A. Willard, E. Brück, C.H. Chen, S.G. Sankar, J.P. Liu, *Adv. Mater.* **23**, 821 (2011).
- [7] T. Graf, C. Felser, S.S.P. Parkin, *Prog. Solid State Chem.* **39**, 1 (2011).
- [8] V.K. Jain, N. Lakshmi, R. Jain, V. Jain, A.R. Chandra, K. Venugopalan, *J. Mater. Sci.* **52**, 6800 (2017).
- [9] X.F. Zhu, L. Wang, *Eur. Phys. J. B* **90**, 64 (2017).
- [10] R. Jain, N. Lakshmi, V. K. Jain, A. R. Chandra, *AIP Conf. Proc.* **1942**, 090011 (2018).
- [11] I. Galanakis, K. Özdoğan, B. Aktaş, *Appl. Phys. Lett.* **89**, 042502 (2006).
- [12] Y. Jirásková, J. Buršík, D. Janičkovič, O. Životský, *Materials* **12**, 710 (2019).
- [13] N.I. Kourov, V.V. Marchenkov, K.A. Belozerovala, H.W. Weber, *J. Exp. Theor. Phys.* **118**, 426 (2014).
- [14] M. Belkhouane, S. Amari, A. Yakoubi, A. Tadjer, S. Méçbih, G. Murtaza, S. Bin Omran, R. Khenata, *J. Magn. Magn. Mater.* **377**, 211 (2015).
- [15] V.K. Jain, N. Lakshmi, R. Jain, A.R. Chandra, *J. Supercond. Nov. Magn.* **32**, 739 (2018).
- [16] F. Dahmane, Y. Mogulkoc, B. Doumi, A. Tadjer, R. Khenata, S.B. Omran, D.P. Rai, G. Murtaza, D. Varshney, *J. Magn. Magn. Mater.* **407**, 167 (2016).
- [17] Z.H. Liu, X.Q. Ma, F.B. Meng, G.H. Wu, *J. Alloys Comp.* **509**, 3219 (2011).
- [18] V.K. Jain, N. Lakshmi, V. Jain, A.K. Sijo, K. Venugopalan, *AIP Conf. Proc.* **1665**, 130032 (2015).
- [19] A. Vinesh, H. Bhargava, N. Lakshmi, K. Venugopalan, *J. Appl. Phys.* **105**, 07A309 (2009).
- [20] N.I. Kourov, V.V. Marchenkov, A.V. Korolev, L.A. Stashkova, S.M. Emel'yanova, H.W. Weber, *Phys. Solid State* **57**, 700 (2015).
- [21] H. Ebert, D. Ködderitzsch, J. Minár, *Rep. Prog. Phys.* **74**, 096501 (2011).
- [22] J.P. Perdew, K. Burke, M. Ernzerhof, *Phys. Rev. Lett.* **77**, 3865 (1996).
- [23] A.I. Liechtenstein, M.I. Katsnelson, V.P. Antropov, V.A. Gubanov, *J. Magn. Magn. Mater.* **67**, 65 (1987).
- [24] X.P. Wei, Y.L. Zhang, X.W. Sun, T. Song, P. Guo, Y. Gao, J.L. Zhang, X.F. Zhu, J.B. Deng, *J. Alloys Comp.* **694**, 1254 (2017).
- [25] X.P. Wei, X.W. Sun, T. Song, J.H. Tian, P. Guo, *J. Supercond. Nov. Magn.* **31**, 2797 (2018).

- [26] F.D. Murnaghan, *Am. J. Math.* **59**, 235 (1937).
- [27] V. Alijani, S. Ouadi, G.H. Fecher, J. Winterlik, S.S. Naghavi, X. Kozina, G. Stryganyuk, C. Felser, *Phys. Rev. B* **84**, 224416 (2011).
- [28] S. Skaftouros, K. Özdoğan, E. Şaşıoğlu, I. Galanakis, *Phys. Rev. B* **87**, 024420 (2013).
- [29] I. Galanakis, P.H. Dederichs, N. Papanikolaou, *Phys. Rev. B* **66**, 174429 (2002).
- [30] E. Şaşıoğlu, L.M. Sandratskii, P. Bruno, *Phys. Rev. B* **72**, 184415 (2005).